Journal Pre-proof

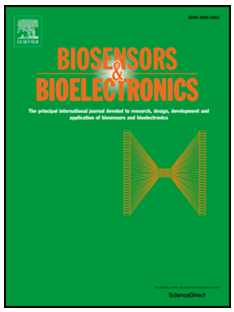

A versatile biomolecular detection platform based on photo-induced enhanced Raman spectroscopy

Tiantian Man, Wei Lai, Mingshu Xiao, Xiwei Wang, Arun Richard Chandrasekaran, Hao Pei, Li Li

PII: S0956-5663(19)30821-8

DOI: https://doi.org/10.1016/j.bios.2019.111742

Reference: BIOS 111742

To appear in: *Biosensors and Bioelectronics*

Received Date: 3 July 2019

Revised Date: 19 August 2019

Accepted Date: 28 September 2019

Please cite this article as: Man, T., Lai, W., Xiao, M., Wang, X., Chandrasekaran, A.R., Pei, H., Li, L., A versatile biomolecular detection platform based on photo-induced enhanced Raman spectroscopy, *Biosensors and Bioelectronics* (2019), doi: https://doi.org/10.1016/j.bios.2019.111742.

Credit Author Statement

A Versatile Biomolecular Detection Platform Based on Photo-Induced Enhanced Raman Spectroscopy

L.L., H.P. and A.C. supervised the project. T.M., W.L., M.X., L.L. and H.P. conceived and designed the experiments. T.M., W.L., M.X. and X. W. performed the experiments. A.C. provided reagents/materials/analysis tools. T.M., W.L., M.X. H.P. and L.L. performed data analysis. T.M., W.L., M.X., L.L. and H.P. wrote the paper, and all authors read and approved the manuscript.

A Versatile Biomolecular Detection Platform Based on Photo-Induced Enhanced Raman Spectroscopy

Tiantian Man[a,#], *Wei Lai*[a,#], *Mingshu Xiao*[a,#], *Xiwei Wang*[a], *Arun Richard Chandrasekaran*[b], *Hao Pei*[a], *and Li Li*[a,*]

[a]Shanghai Key Laboratory of Green Chemistry and Chemical Processes, School of Chemistry and Molecular Engineering, East China Normal University, 500 Dongchuan Road, Shanghai, 200241, P. R. China

[b]The RNA Institute, University at Albany, State University of New York, Albany, NY 12222, USA

[#]These authors contributed equally to this work

Keywords: PIERS effect, biosensor, aptamer, SERS

ABSTRACT: Surface-enhanced Raman spectroscopy (SERS) as one of the effective tools for sensitive and selective detection of biomolecules has attracted tremendous attention. Here, we construct a versatile biomolecular detection platform based on photo-induced enhanced Raman spectroscopy (PIERS) effect for ultrasensitive detection of multiple analytes. In our PIERS sensor, we exploit the molecular recognition capacity of aptamers and the high affinity of aptamers with analyte to trigger TiO_2@AgNP substrates binding with Raman tag-labeled gold nanoparticles probes via analyte, thus forming sandwich complexes. Additionally, combining plasmonic nanoparticles with photo-activated substrates allows PIERS sensor to achieve increased sensitivity beyond the normal SERS effect upon ultraviolet irradiation. Accordingly, the PIERS can be implemented for analysis of multiple analytes by designing different analyte aptamers, and we further demonstrate that the constructed PIERS sensor can serve as a versatile detection platform for sensitively analyzing various biomolecules including small molecules (adenosine triphosphate (ATP), limit of detection (LOD) of 0.1 nM), a biomarker (thrombin, LOD of 50 pM),

and a drug (cocaine, LOD of 5 nM). Therefore, this versatile biomolecular detection platform based on PIERS effect for ultrasensitive detection of multiple analytes holds great promise to be a practical tool.

1. Introduction

Surface-enhanced Raman spectroscopy (SERS), compared with normal Raman spectroscopy, enormously increases Raman signals with factors up to 10^{14}, which results from the strong light-induced electric field within localized nanostructured space (entitled “hot spots”) (Yoon et al., 2008; He et al., 2011), offering possibility of developing ultrasensitive SERS-based biosensors (Cao et al., 2002; Chen et al., 2008; Qian et al., 2008; Wang et al., 2012; Qu et al., 2017; Su et al., 2017). As a nondestructive and noninvasive technique, SERS requires minimal sample amount for testing. In addition, its minimized background signal, peak overlapping and photobleaching make SERS widely used in biological systems (Pallaoro et al., 2010; Ko et al., 2013; Ye et al., 2013; Fu et al., 2016). Owing to the scattering amplification on the surface of nanoscale roughened noble metal substrates, SERS also has shown promising potential as a powerful analytical tool to yield molecular fingerprints and with good sensitivity (Zhao et al., 2014). Meantime, the SERS technique presents broad biological applications, including the detection of nucleic acid (Barhoumi and Halas 2010; Langlet et al., 2011; Shen et al., 2012; Chen et al., 2017; Qi et al., 2017), proteins (Chen et al., 2008; Chen et al., 2013), small molecules (Kim et al., 2016), heavy metallic ions (Wang et al., 2010; Miao et al., 2017; Qi et al., 2017; Qu et al., 2017), and cells (Ramya et al., 2016) due to its high sensitivity and selectivity, which makes it a viable alternative to fluorescence detection methods (Li et al., 2007; He et al., 2010; Li et al., 2010; Ge et al., 2011; Yang et al., 2014; Chen, Chao et al., 2017; Zhong et al., 2018). For instance, recent studies by Hepel et al. developed a plasmonic nanocarrier grid-enhanced Raman sensor with well-controlled hot spots for studying the anticancer drug delivery and testing the anticancer drug interactions with DNA in

biological environment (Ilkhani et al., 2016; Kurzątkowska et al., 2017).

It is commonly known that gold nanoparticles (AuNPs) and silver nanoparticles (AgNPs) are considered as well-established SERS substrates for biomolecule detection. On the other hand, tremendous efforts also have been devoted to studying semiconductor materials as SERS substrates (Kim et al., 2009; Musumeci et al., 2009; Wang et al., 2012). For instance, Yang group developed a recyclable SERS-active substrate composed of Au coated TiO_2 nanotube arrays for multifold organic pollutants detection (Li, Chen et al., 2010). However, previous research has revealed that incorporating metallic nanoparticles onto these non-active substrates is inferior to the metallic nanoparticles alone in terms of SERS signal (Sudnik et al., 1996; Ng et al., 2016), which hinders work on the incorporation of semiconductor on active SERS substrates for enhancement (Liu et al., 2006). Recently, Ivan P. Parkin group proposed photo-induced enhanced Raman spectroscopy (PIERS), wherein photo-excitation of TiO_2 gives rise to strong Raman enhancement at the metallic nanoparticles sites, increasing sensitivity beyond the traditional SERS effect (Ben-Jaber et al., 2016). For instance, Zhang et al. developed a three-dimensional TiO_2-Ag nanopore arrays with excellent trace amount detection ability for toxic organics based on PIERS effect (Zhang et al., 2019). Nevertheless, despite the recent progress, to the best of our knowledge, the PIERS technique has not yet been applied to biomolecular detection.

In this work, we constructed a versatile biomolecular detection platform based on PIERS effect for ultrasensitive detection of multiple analytes. By combining plasmonic nanoparticles with photo-activated substrates, the PIERS-based sensor achieved increased sensitivity beyond the normal SERS effect upon ultraviolet irradiation. As shown in Figure 1a, TiO_2 substrate was prepared through TiO_2 nanostructure grown on Ti foil with hydrothermal method, followed by deposition of AgNPs on TiO_2 substrate (TiO_2@AgNP) using magnetic sputtering (MS). Thereafter, we took three steps to construct the biomolecular detection platform (Figure 1b). The

first step was to modify the as-prepared TiO_2@AgNP with single strand DNA (ssDNA1). Following, the modified TiO_2@AgNP was immersed in a mixture solution containing Raman tag (4-MBA)-labeled AuNPs-ssDNA2 probes (Au-ssDNA2-4-MBA) and analytes in step 2. Notably, ssDNA1 was attached to the TiO_2@AgNP substrates via silver-sulfur chemistry and ssDNA2 linked with AuNPs via gold-sulfur chemistry. Additionally, both ssDNA1 and ssDNA2 were designed as aptamer of analyte. Aptamers, working as molecular recognition elements here, have high affinity with analyte. Accordingly, the presence of analyte facilitated AuNPs-ssDNA2 binding with DNA1-modified TiO_2@AgNP substrates and thus formed an associated sandwich complex (Zuo et al., 2009). Then, pre-irradiation with ultraviolet light results in the formation of oxygen vacancy (V_O) defects on TiO_2 surfaces which produce donor states at ~0.7 eV below the TiO_2 conduction band edge. Upon Raman laser irradiation, electrons would be prompted from V_O defects states into the TiO_2 conduction band, followed by electron migration from TiO_2 into Ag energy levels. Accordingly, such PIERS effect induces enhanced Raman scattering at AgNPs and AuNPs sites in step 3. In addition, both the long lifetime of PIERS phenomenon (Figure 1b) and the enhanced EM-fields between AuNPs and AgNPs (Figure 1c) further contributed to the increased sensitivity of PIERS sensors. Hence, this detection platform with ultraviolet light-induced PIERS effect beyond normal SERS effect provides possibilities for quantitative interrogation of the relationship between analyte and Raman signal. It should be pointed out that our PIERS sensor can achieve multiple analytes detection by designing different analyte aptamers. Therefore, this versatile biomolecular detection platform based on PIERS increasing SERS effect is expected for ultrasensitive detection of multiple analytes.

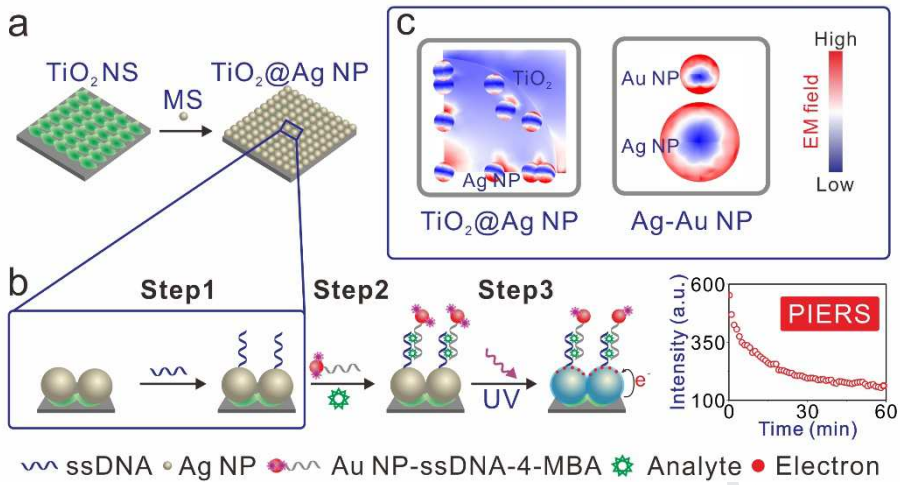

Figure 1. The construction of biomolecular detection platform based on PIERS. (a) The preparation of TiO_2@AgNP substrate by magnetic sputtering (MS). (b) The construction of PIERS sensor for analyte detection, and the right panel shows a time-dependent PIERS signal on TiO_2NF@AgNP substrate after ultraviolet irradiation. (c) The simulated EM-fields intensity distribution of TiO_2@AgNP and Ag-Au.

2. Experimental

2.1. Chemical and reagent

α-thrombin, guanosine triphosphate (GTP), cytidine triphosphate (CTP) and adenosine triphosphate (ATP) were purchased from HeFei BoMei Biotechnology Co., Ltd. (Hefei, China). Uridine triphosphate (UTP) was purchased from Shanghai Yuanye Bio-Technology Co., Ltd. (Shanghai, China). Adenosine diphosphate (ADP), adenosine monophosphate (AMP) and 4-mercaptobenzoic acid (4-MBA) were purchased from Sigma-Aldrich (St. Louis, MO, USA) and used without further purification. The oligonucleotides were provided by Sangon Biotech Co., Ltd (Shanghai, China) and the sequence of oligonucleotides were listed in the Table S1. All aqueous solutions were prepared using deionized (DI) water with a resistivity of 18.2 $M\Omega \cdot cm^{-1}$ obtained from a Millipore system for all experiments. All chemicals were the analytical grade and used as received.

2.2. Characterization

The MS of AgNPs on the TiO_2 substrate was conducted with a High vacuum magnetron sputtering system (JGP450, Shenyang Science Instrument Co., Ltd.). The crystal structure of TiO_2 was investigated by X-ray diffraction (XRD) using a Bruker-AXS Micro diffractometer (Model D5005). The morphologies, composition, and structure of the samples were investigated by a Hitachi S-4800 scanning electron microscopy (SEM), energy-dispersive X-ray spectroscope (EDS), and a JEOL JEM-2100 transmission electron microscopy (TEM), respectively. Raman spectra were acquired using a DXR intelligent Raman spectrometer (Thermo Scientific, America) equipped with a 780 nm-laser (HeNe, 49.995 mW). And the Raman spectra were collected using a 10 × objective lens (N.A. = 0.25).

2.3. Calculation

To investigate the role of strong electromagnetic enhancement of the AgNPs, AuNPs, and Ag-Au, the local electric field intensity distributions around AgNPs, AuNPs, and Ag-Au were simulated by the commercial software COMSOL Multiphysics based on a finite element method (FEM, COMSOL Multiphysics 4.3) under irradiation of a monochromatic light at 780 nm. In these calculations, the AuNP was modeled as a ball with a radius of 12.5 nm and the AgNP was modeled as a ball with a radius of 25 nm. TiO_2 nanorod (TiO_2NR) was modeled as an ellipsoid. TiO_2 NRs had an aspect ratio of 4.18 with a short axis radius of 38.5 nm and a long axis radius of 161 nm. TiO_2 nanoflower (TiO_2NF) was modeled as a petal with a radius of 112 nm. The permittivity data of gold used here are obtained from the bulk experimental result of Johnson and Christy (Johnson and Christy, 1972).

2.4. Preparation of TiO_2 nanostructures

The TiO_2 substrate was prepared with a hydrothermal method (Wang et al., 2011). Typically, Ti foils were successively cleaned by sonication in DI water, acetone, and DI water. To remove the TiO_2 film on the surface of Ti foil, the Ti foil was immersed

into the diluted HF solution for ten seconds, followed by cleaning with DI water and dried in a nitrogen gas flow. Subsequently, the treated Ti foil was placed into a Teflon-sealed autoclave and immersed in 15 mL of 5 M NaOH solution. Thereafter, the autoclave was put in a preheated electric oven at 170 °C for 16 h. After the autoclave was naturally cooled to room temperature, the sample was washed with DI water. To obtain the anatase TiO_2, the products mentioned above were placed in the Teflon-sealed autoclave loaded with 15 mL DI water at 170 °C for 3 h. After cooling to room temperature and washed with DI water, the products turned white, indicating that the TiO_2NFs have been successfully prepared.

Meanwhile, the TiO_2 NRs were also synthesized using hydrothermal method. Similar to the synthetic route of TiO_2NFs, the hydrothermal process for TiO_2 NRs were conducted at 170 °C for 20 h and corresponding hydrolysis process was performed at 150 °C for 5 h. Finally, the as-prepared substrate exhibited pale white color.

2.5. Preparation of TiO_2@AgNP

The AgNPs were sputtered on the TiO_2 substrates (TiO_2NFs or TiO_2NRs) mentioned above through MS with a deposition rate of 2 $Å \cdot s^{-1}$. Finally, AgNPs with a diameter of 50 nm appeared on the TiO_2NFs or TiO_2NRs substrate (TiO_2@AgNP).

2.6. Preparation of ssDNA1-modified TiO_2@AgNP

To prepare ssDNA1-modified TiO_2@AgNP, the as-prepared TiO_2@AgNP was immersed into 5 mL 10 mM PBS (pH 7.4) containing 5 μM ssDNA1 for 2 h. In this step, TiO_2@AgNP was modified with ssDNA1 via the well-known silver-sulfur chemistry. Thereafter, ssDNA1-functioned TiO_2@AgNP was washed with 10 mM PBS for three times to remove nonspecifically bound ssDNA1 and incubated in 10 mM PBS buffer prior to use.

2.7. Preparation of Raman tag-labeled AuNPs-ssDNA2 probe

25 nm AuNPs were pre-synthesized by citrate reduction of $HAuCl_4$ according to

the reported procedure with some modification (Hill and Mirkin 2006). Briefly, 50 mL 38.8 mM trisodium citrate solution was added to a boiling, rapidly stirred solution of 1 mM $HAuCl_4$. The solution was kept boiling and stirred until the solution turned from yellow to deep red. After being cooled to room temperature, the prepared AuNPs were stored at 4 °C.

For the AuNPs-ssDNA2 probe preparation (Zhang et al., 2012), 2 μL of 100 μM ssDNA2 and 10 μL of 500 mM citrate-HCl buffer (pH 3.0) were added into 500 μL 10 nM AuNPs, and incubated for 20 min. Then, the mixture was centrifuged (10 000 rpm, 15 min, 15 °C) to remove the free ssDNA2 and the precipitate was re-dispersed with 10 mM PBS. The procedure was repeated for three times. The yielded AuNPs-ssDNA2 probe was re-dispersed in 10 mM PBS and stored at 4 °C for further use. Following, a certain amount of 4-MBA was added into the as-prepared AuNPs-ssDNA2 probe solution to absorb on AuNPs surface, and then the mixture was incubated for overnight under gentle shaking. Finally, after the mixed solution mentioned above was centrifuged to remove excess 4-MBA and washed with 10 mM PBS for three times, Raman tag-labeled AuNPs-ssDNA2 probes were suspended in 10 mM PBS for further use.

2.8. PIERS Sensor for ATP Detection

For ATP detection, the ssDNA1-modified TiO_2@AgNP was immersed in a mixture of Raman tag-labeled AuNPs-ssDNA2 probe (10 nM) and various concentrations (0-1 μM) of ATP and incubated for 30 min. Subsequently, the PIERS sensor was rinsed with 10 mM PBS, and allowed to dry in air. The constructed PIERS sensor was then irradiated under ultraviolet light (365 nm, handheld ultraviolet analyzer ZF-5C, 2 × 6 W bulbs) with a distance of 10 cm to the samples for 30 min. Thereafter, the Raman spectra were obtained from treated TiO_2 substrates for an accumulation time of 10 s. Three spectra from different sites were tested from each sample.

2.9. PIERS Sensor for Thrombin or Cocaine Detection

For thrombin detection, the ssDNA3-modified TiO_2@AgNP was immersed in a mixture of Raman tag-labeled AuNPs-ssDNA4 probe (10 nM) and various concentrations (0-1 μM) of thrombin and incubated for 30 min. For cocaine detection, the ssDNA5-modified TiO_2@AgNP was immersed in a mixture of Raman tag-labeled AuNPs-ssDNA6 probe (10 nM) and various concentrations (0-10 μM) of thrombin and incubated for 30 min. Subsequently, the PIERS sensor was rinsed with 10 mM PBS, and allowed to dry in air, followed by irradiation under ultraviolet light (365 nm) for 30 min. Thereafter, the Raman spectra were obtained from treated TiO_2 substrates for an accumulation time of 10 s. Three spectra from different sites were tested from each sample.

3. Results and discussion

3.1. Preparation of Raman substrate

Given that TiO_2 is commonly used as semiconductor substrate due to its excellent optical property (Barborini et al., 2005; Ng et al., 2010), we firstly synthesized two types of TiO_2 nanostructures using hydrothermal method. The SEM images (Figure 2a, b) confirm that two types of TiO_2 nanostructures (TiO_2NF and TiO_2NR) with different morphologies were yielded. Subsequently, the composition of TiO_2 NF was analyzed with EDS. Atomic percentage from EDS elemental analysis (Figure 2c) are found to be 9.08%, 61.86%, and 29.07% for C, O, and Ti, respectively, confirming the ratio of O to Ti is close to 2:1. Additionally, the treated Ti foil was characterized by XRD to further identify the material composition. The XRD pattern (Figure 2d) exhibits the diffraction peak at $2\theta = 38.0°$ ascribed to Ti foil and the peaks at $2\theta = 40.8°$, 53.0°, and 70.7° assigned to TiO_2, coinciding with the standard diffraction pattern of anatase TiO_2 (Nian and Teng 2006; Baker and Kamat 2009).

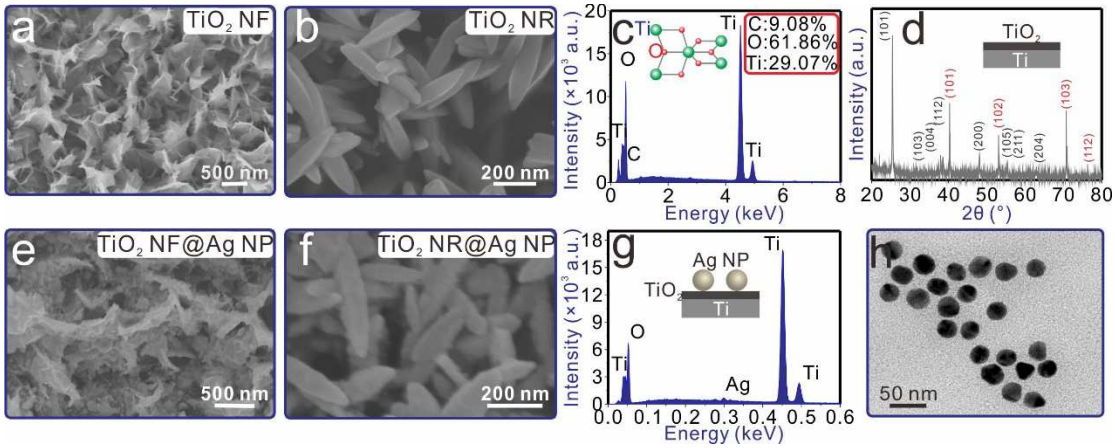

Figure 2. Characterization of the Raman substrate. The SEM images of (a) TiO_2NF and (b) TiO_2NR. (c) The EDS and (d) the XRD pattern of TiO_2NF. The SEM images of (e) TiO_2NF@AgNP and (f) TiO_2NR@AgNP. (g) The EDS pattern of TiO_2NF@AgNP substrate. (h) The TEM image of AuNPs.

To enhance the SERS performance of substrates, we took advantage of MS method to sputter the AgNPs (~50 nm) on the TiO_2 substrates. After sputtering, the treated TiO_2NF and TiO_2NR exhibited deep blue and brown color, respectively. Following, their morphologies were recorded with SEM. As observed from Figure 2e and f, numerous nanoparticles were attached to TiO_2 substrates and made the substrates roughness, indicating that Ag-coated TiO_2NF (TiO_2NF@AgNP) and Ag-coated TiO_2NR (TiO_2NR@AgNP) were successfully prepared. Meanwhile, the EDS spectrum (Figure 2g) also revealed that the TiO_2NF@AgNP substrate is composed of Ti, O, and Ag elements. Additionally, in order to carry out further study, we synthesized AuNPs via citrate reduction of $HAuCl_4$. The TEM image (Figure 2h) confirms that the well-dispersed AuNPs around 25 nm were successfully synthesized.

3.2 Raman performance of the PIERS sensor

ATP as cellular energy currency provides energy for various biochemical reactions and regulates cellular metabolism in biological processes (Roseman et al., 2015; Chen, Chao et al., 2017), and is thus considered as an important indicator for cell damage, inhibition and proliferation (Jordan and Wilson 2004; Wei et al., 2015). The ATP level also reflects the degree of microbial contamination (Frundzhyan and Ugarova

2007). Moreover, numerous studies have demonstrated that ATP depletion is associated with many diseases including Parkinson's diseases, hypoglycemia, ischemia and even malignant tumors (Bodzioch et al., 1999; Gourine et al., 2005; Mariathasan et al., 2006). Accordingly, the accurate detection and quantification of ATP is of great importance for disease diagnosis and biochemical research. As a result, ATP is used as model analyte and detected with our PIERS-based biomolecular detection platform.

Prior to irradiation with ultraviolet light, we prepared DNA1-modified TiO_2@AgNP and Raman tag (4-MBA)-labeled AuNPs-DNA2 probe, followed by DNA1-modified TiO_2@AgNP substrates immersed into mixture solution of Raman tag-labeled AuNPs-DNA2 probe and ATP. ATP reassembles DNA1 and DNA2 into the intact aptamer tertiary structure (Zhou et al., 2019), thus inducing the binding of DNA1-modified TiO_2@AgNP and AuNPs-DNA2 probe. Hence, the PIERS sensor has been constructed. As shown in Figure 3a, the working mechanism of our PIERS sensor is based on the electron migration mediated by ultraviolet light from the TiO_2 substrates to the AgNPs (Ben-Jaber, Peveler et al., 2016). Previous study has revealed that V_O defects on substrates could be created through pre-irradiation with ultraviolet light (Mezhenny et al., 2003). It is important to highlight that these resulting V_O defects induce absorption above 500 nm (Lin et al., 2005). Upon Raman laser illumination, electrons migrated from the conduction band of TiO_2 states to the V_O in the PIERS effect were transferred into Ag energy levels (Yoo et al., 2014). To investigate the effect of photo-excitation on SERS performance, we studied the Raman spectra of TiO_2NF@AgNP sensor before and after ultraviolet light irradiation. Observed from Figure 3b, the intensity of Raman signal at 1078 cm^{-1} after irradiation is ~3 times of that without irradiation, indicating that the Raman performance of our PIERS sensor indeed has been enhanced after activation with ultraviolet light pre-irradiation.

Moreover, a decrease in the PIERS signal occurred within 60 min on

TiO_2NF@AgNP substrate after ultraviolet irradiation (Figure 3c), which is attributed to surface healing upon exposure of the substrate to air (Onda et al., 2004). Nevertheless, this long lifetime of our PIERS sensor allows us to assess the sensor performance after TiO_2@AgNP substrate activation with ultraviolet light pre-irradiation. Next, we recorded the Raman mapping of the PIERS sensor at 1078 cm^{-1} to evaluate its reproducibility. Figure 3d shows spatial uniformity of the Raman signal in TiO_2NF@AgNP substrates, which is well consistent with the narrow distribution of the Raman signal intensity. For comparison of SERS performance between two types of TiO_2 nanostructures, the random 10 measurements of PIERS spectra from TiO_2NF@AgNP and TiO_2NR@AgNP were conducted. As seen in Figure 3e, we found that the PIERS performance of TiO_2NF@AgNP is better than that of TiO_2NR@AgNP after ultraviolet light irradiation. Moreover, the signal intensity of TiO_2NF@AgNP at 1078 cm^{-1} is ~2 times of TiO_2NR@AgNP (Figure 3f), and the prominent PIERS performance of TiO_2NF@AgNP over TiO_2NR@AgNP may be ascribed to its high specific surface area (Tian et al., 2008; Chen et al., 2010). Additionally, their corresponding reliability also is acceptable. Taking together these results, TiO_2NF@AgNP was used as substrates for further analysis.

To gain deeper insight of SERS performance of PIERS sensor, we exploited FEM method to carry out a theoretical simulation and calculated the EM-field intensity distribution. As shown in Figure 3g, h and i, the maximum value of EM-field intensity of Ag-Au is ~6 times of TiO_2NR@AgNP and ~4 times of TiO_2NF@AgNP without ultraviolet irradiation, which suggests strong plasmonic coupling for Au-Ag nanoparticles via the bridge connection of ATP. It is noted that the Raman intensity is proportional to the fourth power of the electric field (Moskovits 2005; Theiss et al., 2010). Consequently, the FEM data indicates the high activity of our sensor, which effectively facilitates the increasing of Raman signals.

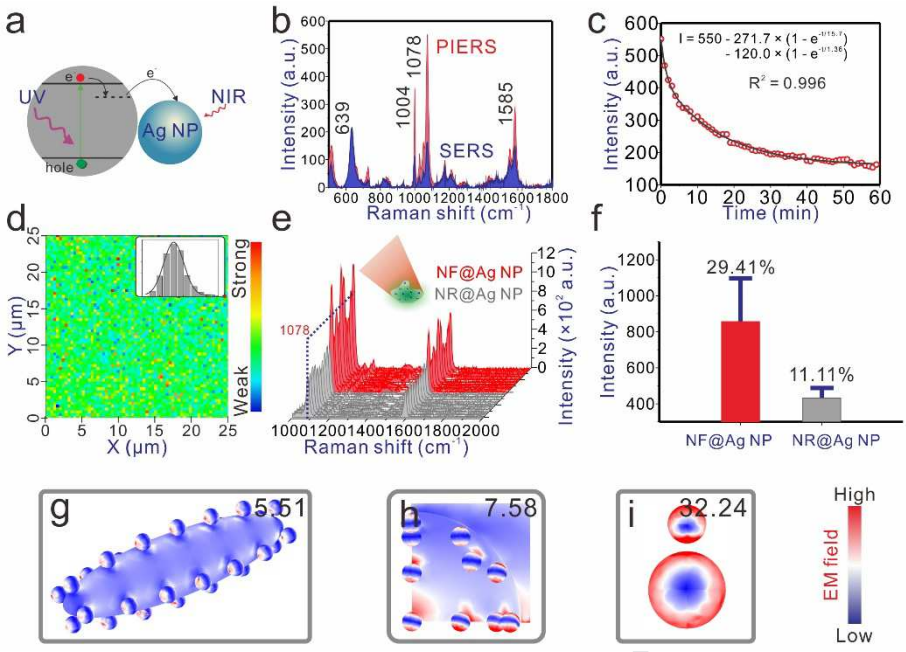

Figure 3. Raman performance of the prepared TiO_2@AgNP substrate. (a) The schematic of PIERS via a charge transfer. (b) The comparison of PIERS spectra and SERS spectra for 4-MBA on TiO_2NF@AgNP substrate. (c) A time-dependent PIERS signal at 1078 cm^{-1} of 4-MBA on TiO_2NF@AgNP substrate after ultraviolet irradiation. (d) Raman mapping of 4-MBA on TiO_2NF@AgNP substrate. Inset: distribution of Raman signal intensity. (e) The random 10 measurements PIERS spectra of 4-MBA on TiO_2NF@AgNP (red line) and TiO_2NR@AgNP (brown line) substrate. (f) The PIERS signal at 1078 cm^{-1} of 4-MBA on TiO_2NF@AgNP (red) and TiO_2NR@AgNP (brown) substrate. The simulated EM-fields intensity distribution of (g) TiO_2NR@AgNP, (h) TiO_2NF@AgNP and (i) Ag-Au nanoparticles.

3.3 PIERS sensor for ATP detection

According to previous studies (Zuo, Xiao et al., 2009; Kashefi-Kheyrabadi and Mehrgardi 2012), ATP binding aptamer, a 27-base single DNA, could be split into two segments of 13-base, 3' (DNA1) and 14-base, 5' (DNA2), to construct a sandwich apta-sensor for ATP detection, wherein ATP molecules were immobilized via two segments of ATP aptamer folding around ATP molecules and forming an associated complex, a G-quarter structure (Huizenga and Szostak 1995). The details on the binding mechanism are illustrated in Figure S1. On the basis of these findings, we

used DNA1 and DNA2 to modify TiO_2NF@AgNP and 4-MBA-labeled AuNPs, respectively. Observed from Figure 4a, DNA1-modified TiO_2NF@AgNP and DNA2-modified AuNPs probes would capture ATP molecules on the dependence of the high affinity of aptamers and ATP molecules, inducing TiO_2NF@AgNP binding with AuNPs-ssDNA2 probes. In addition, we characterized the morphologies of the TiO_2NF@AgNP substrate after the assay. No obvious morphological changes of the TiO_2NF@AgNP was observed and the AuNPs were found to be dispersed on AgNPs (Figure S2), suggesting AuNPs binding to TiO_2NF@AgNP as expected. As a result, the Au probes with 4-MBA reporter were immobilized on the TiO_2NF@AgNP substrate, and a PIERS sensor for ATP detection thus has been constructed.

Next, we exploited the constructed PIERS sensor to detect ATP molecules. Figure 4b presents the response of the PIERS sensor to the different ATP concentrations. We found the Raman intensity as a function of ATP concentration, indicating that more 4-MBA labeled-AuNPs probes were bound onto TiO_2NF@AgNP substrate with the addition of more ATP molecules. Thereafter, the PIERS band intensities versus ATP concentration on a logarithmic scale were further summarized. As shown in Figure 4c, the intense PIERS peak at 1078 cm^{-1} in the spectra is used as a calibration band, and the intensity is linearly correlated to ATP concentration on a logarithmic scale ranging from 1 μM to 0.1 nM. In addition, the LOD of our PIERS sensor was determined to be 0.1 nM, which is lower than previous electrochemical (Zuo et al., 2007; Kashefi-Kheyrabadi and Mehrgardi 2012; Liu et al., 2014) and fluorescent methods (Kim et al., 2010; Liu et al., 2014; Wang et al., 2015; Wei, Chen et al., 2015), comparable to or lower than SERS methods (Ye, Xiao et al., 2013; Xu et al., 2017) (see Table S2). The low LOD that our PIERS sensor exhibited can be attributed to: i) photo-induced activation, ii) hot spot between AgNPs and AuNPs, and iii) the high affinity of aptamers with ATP.

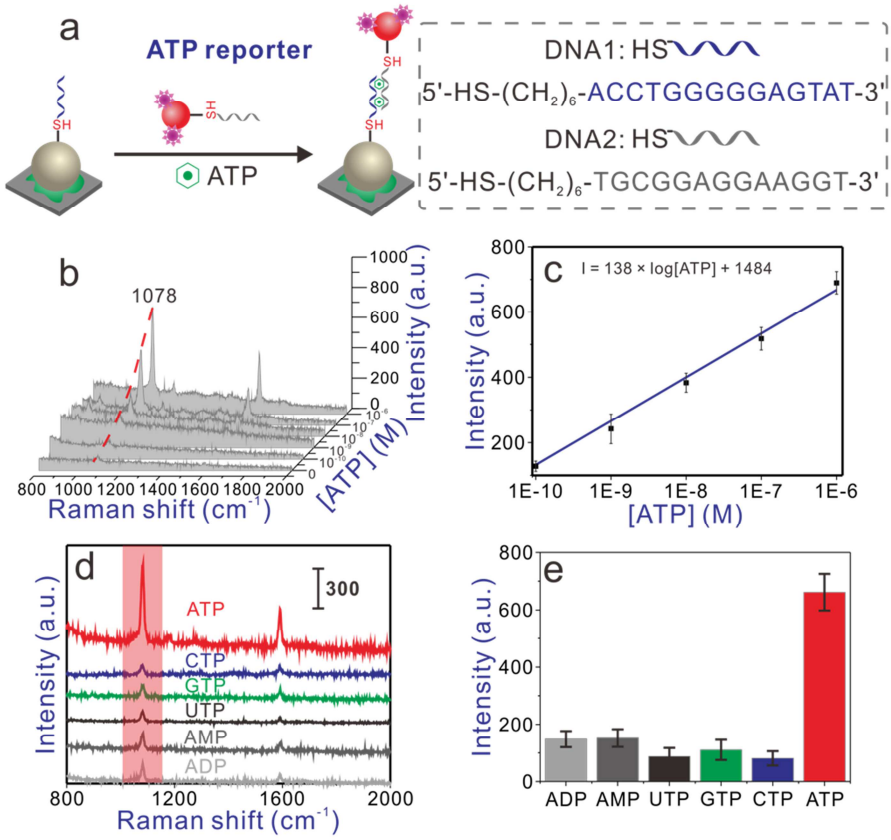

Figure 4. PIERS sensor for ATP detection. (a) The schematic of PIERS sensor for ATP detection. (b) PIERS spectra of 4-MBA with different concentrations of ATP. (c) The linear range of PIERS sensor response to ATP at 1078 cm^{-1} of 4-MBA. (d) Selectivity of the PIERS spectra with ATP and ATP analogs. (e) The PIERS signal at 1078 cm^{-1} of 4-MBA for ATP detection compared to ATP analogs.

In order to evaluate our PIERS sensor for specific detection of ATP, control experiments were carried out. As presented in Figure 4d, even 10 μM typical ATP analogs showed much weaker responses than ATP with 1 μM, which suggests the good specificity of our system for ATP detection. Notably, the good selectivity of the sensor shown in Figure 4d and e can be ascribed to the specific recognition ability of aptamers towards ATP. Taking together these results, our PIERS sensor based on photo-excitation increasing SERS effect exhibits high sensitivity and selectivity for ATP detection.

3.4 PIERS sensor for anti-thrombin and cocaine detection

To broaden the application of our detection platform, we exploited this PIERS sensor to detect other analytes. As one of the most commonly studied proteins, thrombin was chosen as the next molecular target. Accordingly, we took place of the DNA probe with an anti-thrombin aptamer sequence (Pei et al., 2010). As described in Figure 5a, two anti-thrombin aptamers (DNA3 and DNA4), which formed G-quartet structures and bound to different domains of anti-thrombin, were designed to modify TiO_2NF@AgNP and AuNPs, respectively. In addition to molecular recognition elements, anti-thrombin aptamer also has high affinity with anti-thrombin. Thus, the presence of thrombin induced DNA3-modified TiO_2NF@AgNP binding with DNA4-modified AuNPs probes, forming a "sandwich assay". As a result, the constructed PIERS sensor was allowed to detect thrombin. As presented in Figure S3a and Figure 5b, we found that this PIERS sensor also exhibited excellent sensitivity toward thrombin, showing a wide linear range from 1 μM to 50 pM and a remarkable detection limit of 50 pM, which is comparable to or lower than the previous SERS methods (Cho et al., 2008; Hu et al., 2008; Bai et al., 2013) (see Table S3). Moreover, this thrombin sensor also shows good selectivity over other analogs (Figure S5a).

Consequently, we believe that PIERS sensor may provide a versatile platform for detection of a broad range of biomolecules by the combination of aptamers. To further confirm this, we took advantage of the PIERS-based platform to detect cocaine which is one of the most studied drugs. The cocaine binding aptamer, a 32-base single aptamer, was split into 12-base, 5' (DNA5) and 20-base, 3' (DNA6) based on previous report (Zuo, Xiao et al., 2009). Similarly, TiO_2NF@AgNP and AuNPs were modified with DNA5 and DNA6, two segments of cocaine binding aptamer, respectively. The presence of cocaine could induce the association of DNA5-modied TiO_2NF@AgNP and DNA6-modified AuNPs, forming a three-way junction in which cocaine binding site is located in the lipophilic cavity (Stojanovic et al., 2001) shown in Figure 5c. The details on the binding mechanism are further illustrated in Figure S4. As expected in Figure S3b and Figure 5d, it is found that the PIERS intensity is linearly correlated to cocaine concentration on a logarithmic scale in the range from 10 μM to 5 nM and its

corresponding LOD is 5 nM, which is lower than the previous SERS methods (Chen, Jiang et al., 2008; Yang et al., 2011; Zhao, Shen et al., 2014) (see Table S4). In addition to its high sensitivity, our detection platform also enables specific detection of cocaine (Figure S5b). Note that our detection sensitivity can be further improved when combined with strategies of signal amplification and/or rational designed nanostructures that could achieve high light-use efficiency, for instance, 3D photonic crystals that can function as efficient optical antennas, and areoles arrays with high surface area (Shen, Li et al., 2012; Yang et al., 2015; Li et al., 2018). Given these results, our prepared PIERS sensor could be used as a versatile detection platform.

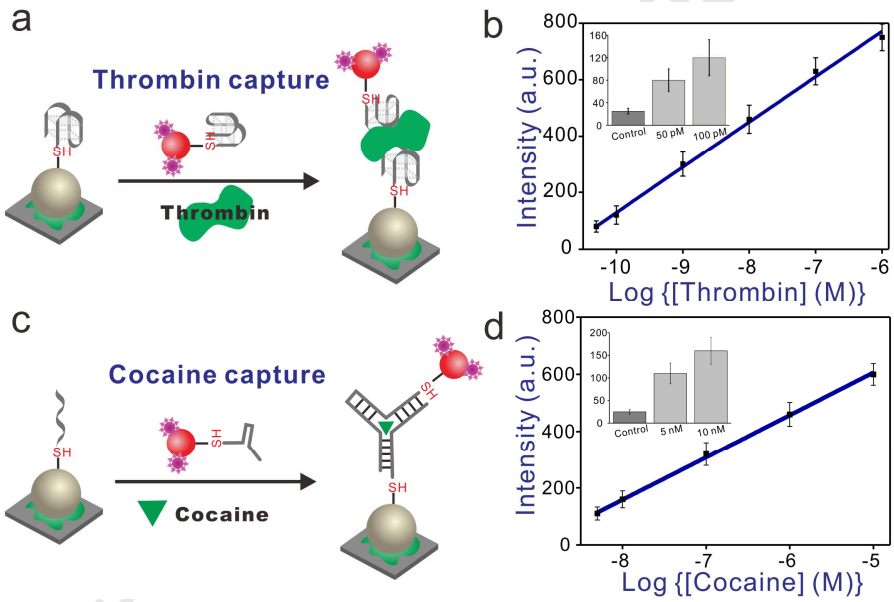

Figure 5. PIERS sensor for anti-thrombin and cocaine detection. (a) The schematic of PIERS sensor for anti-thrombin detection. (b) The linear range of PIERS sensor response to anti-thrombin. Inset: PIERS detection of thrombin in the low concentration range. (c) The schematic of PIERS sensor for cocaine detection. (d) The linear range of PIERS sensor response to cocaine. Inset: PIERS detection of cocaine in the low concentration range.

We also carried out recovery experiments to verify the reliability and feasibility of our sensing platform for practical assays, in which different concentrations of targets were added into the 100-fold diluted healthy human real serum samples. We

discovered that the recovery in serum samples ranges from 95.7% to 105.4% with RSD values ranging from 2.6 to 4.8% (Table S5, S6, and S7), indicating the feasibility of this versatile detection platform for clinical analysis. In biological and biomedical analysis, nonspecific protein adsorption might be an important factor influencing the detection performance of biosensors (Stobiecka 2014). For example, the plasmonic fields in noble metal nanostructures can be modulated by the dielectric function of the protein shell, resulting in a decrease in the SERS efficiency (Stobiecka and Chalupa 2015). In our system, assembly of both oligo (ethylene glycol)-terminated thiols and thiolated DNA probes on AuNPs or AgNPs can be utilized to address this issue because of the nonfouling property of oligo (ethylene glycol) that can repel nonspecific adsorption of proteins in complex systems (Zhang et al., 2008; Wan et al., 2010; Wan et al., 2013). Based on the above results, it is anticipated that our PIERS sensor as a versatile detection platform can be applied for practical analysis.

4. Conclusions

In summary, a versatile biomolecular detection platform based on PIERS effect has been constructed for ultrasensitive detection of multiple analytes. The PIERS sensor for biomolecular detection provides several advantages. First of all, the PIERS sensor can be rapidly and reliably developed, just relying on the molecular recognition capacity of aptamers and the high affinity of aptamers with analyte to trigger TiO_2@AgNP substrates binding with Raman tag-labeled AuNPs probes. Second, the combination of plasmonic nanoparticles with photo-activated substrates enables our PIERS sensor with improved sensitivity beyond the normal SERS effect upon ultraviolet light irradiation. Finally, the PIERS sensor can serve as a versatile detection platform for sensitively detecting various biomolecules including small molecules (ATP, LOD of 0.1 nM), a biomarker (anti-thrombin, LOD of 50 pM), and a drug (cocaine, LOD of 5 nM). The good specificity and high sensitivity of our PIERS sensor are ascribed to: i) photo-induced activation, ii) hot spot between AgNPs and

AuNPs, and iii) the high affinity of aptamers with analytes. Given its various advantages including simplicity, low cost, and multiple analytes detection, this versatile biomolecular detection platform shows promising potential for practical use.

Corresponding author

*E-mail: lli@chem.ecnu.edu.cn.

Acknowledgments

This work was supported by the National Natural Science Foundation of China (Grant No. 21722502), Shanghai Science and Technology Committee (STCSM) (Grant No. 18490740500, Rising-Star Program Grant No. 19QA1403000). L. L. also acknowledges the financial support from the “1000 Youth Talents Plan”.

Appendix A. Supplementary data

Supplementary data to this article can be found online.

References

Bai, Y., Feng, F., Zhao, L., Wang, C., Wang, H., Tian, M., Qin, J., Duan, Y., He, X., 2013. Biosens. Bioelectron. 47, 265-270.

Baker, D.R., Kamat, P.V., 2009. Adv. Funct. Mater. 19 (5), 805-811.

Barborini, E., Conti, A.M., Kholmanov, I., Piseri, P., Podestà, A., Milani, P., Cepek, C., Sakho, O., Macovez, R., Sancrotti, M., 2005. Adv. Mater. 17 (15), 1842-1846.

Barhoumi, A., Halas, N.J., 2010. J. Am. Chem. Soc. 132 (37), 12792-12793.

Ben-Jaber, S., Peveler, W.J., Quesada-Cabrera, R., Cortés, E., Sotelo-Vazquez, C., Abdul-Karim, N., Maier, S.A., Parkin, I.P., 2016. Nat. Commun. 7, 12189.

Bodzioch, M., Orsó, E., Klucken, J., Langmann, T., Böttcher, A., Diederich, W., Drobnik, W., Barlage, S., Büchler, C., Porsch-Özcürümez, M., 1999. Nat. Genet. 22 (4), 347-351.

Cao, Y.C., Jin, R., Mirkin, C.A., 2002. Science 297 (5586), 1536-1540.

Chen, J., Jiang, J., Gao, X., Liu, G., Shen, G., Yu, R., 2008. Chem-Eur. J. 14 (27), 8374-8382.

Chen, J.S., Tan, Y.L., Li, C.M., Cheah, Y.L., Luan, D., Madhavi, S., Boey, F.Y.C., Archer, L.A.,

Lou, X.W., 2010. J. Am. Chem. Soc. 132 (17), 6124-6130.

Chen, L., Chao, J., Qu, X., Zhang, H., Zhu, D., Su, S., Aldalbahi, A., Wang, L., Pei, H., 2017. ACS Appl. Mater. Interfaces 9 (9), 8014-8020.

Chen, L., Fu, X., Li, J., 2013. Nanoscale 5 (13), 5905-5911.

Chen, Z., Tabakman, S.M., Goodwin, A.P., Kattah, M.G., Daranciang, D., Wang, X., Zhang, G., Li, X., Liu, Z., Utz, P.J., 2008. Nat. Biotechnol. 26 (11), 1285-1292.

Cho, H., Baker, B.R., Wachsmann-Hogiu, S., Pagba, C.V., Laurence, T.A., Lane, S.M., Lee, L.P., Tok, J.B.-H., 2008. Nano Lett. 8 (12), 4386-4390.

Frundzhyan, V., Ugarova, N., 2007. Luminescence 22 (3), 241-244.

Fu, X., Cheng, Z., Yu, J., Choo, P., Chen, L., Choo, J., 2016. Biosens. Bioelectron. 78, 530-537.

Ge, Z., Pei, H., Wang, L., Song, S., Fan, C., 2011. Sci. China Chem. 54 (8), 1273-1276.

Gourine, A.V., Llaudet, E., Dale, N., Spyer, K.M., 2005. Nature 436 (7047), 108-111.

He, S., Song, B., Li, D., Zhu, C., Qi, W., Wen, Y., Wang, L., Song, S., Fang, H., Fan, C., 2010. Adv. Funct. Mater. 20 (3), 453-459.

He, Y., Su, S., Xu, T., Zhong, Y., Zapien, J.A., Li, J., Fan, C., Lee, S.-T., 2011. Nano Today 6 (2), 122-130.

Hill, H.D., Mirkin, C.A., 2006. Nat. Protoc. 1 (1), 324-336.

Hu, J., Zheng, P.-C., Jiang, J.-H., Shen, G.-L., Yu, R.-Q., Liu, G.-K., 2008. Anal. Chem. 81 (1), 87-93.

Huizenga, D.E., Szostak, J.W., 1995. Biochemistry 34 (2), 656-665.

Ilkhani, H., Hughes, T., Li, J., Zhong, C.J., Hepel, M., 2016. Biosens. Bioelectron. 80, 257-264.

Johnson, P.B., Christy, R.-W., 1972. Phys. Rev. B 6 (12), 4370-4379.

Jordan, M.A., Wilson, L., 2004. Nat. Rev. Cancer. 4 (4), 253-265.

Kashefi-Kheyrabadi, L., Mehrgardi, M.A., 2012. Biosens. Bioelectron. 37, 94-98.

Kim, D.J., Jeon, T.Y., Baek, Y.-K., Park, S.-G., Kim, D.-H., Kim, S.-H., 2016. Chem. Mater. 28 (5), 1559-1565.

Kim, J.H., Ahn, J.H., Barone, P.W., Jin, H., Zhang, J., Heller, D.A., Strano, M.S., 2010. Angew. Chem. Int. Ed. 49 (8), 1456-1459.

Kim, K., Lee, Y.M., Lee, H.B., Shin, K.S., 2009. Biosens. Bioelectron. 24, 3615-3621.

Ko, J., Lee, S., Lee, E.K., Chang, S.-I., Chen, L., Yoon, S.-Y., Choo, J., 2013. Phy. Chem. Chem. Phy. 15 (15), 5379-5385.

Kurzątkowska, K., Santiago, T., Hepel, M., 2017. Biosens. Bioelectron. 91, 780-787.

Langlet, M., Sow, I., Briche, S., Messaoud, M., Chaix-Pluchery, O., Dherbey-Roussel, F., Chaudouët, P., Stambouli, V., 2011. Surf. Sci. 605 (23-24), 2067-2072.

Li, D., Shlyahovsky, B., Elbaz, J., Willner, I., 2007. J. Am. Chem. Soc. 129 (18), 5804-5805.

Li, H., Yang, Q., Hou, J., Li, Y., Li, M., Song, Y., 2018. Adv. Funct. Mater. 28 (21), 1800448.

Li, X., Chen, G., Yang, L., Jin, Z., Liu, J., 2010. Adv. Funct. Mater. 20 (17), 2815-2824.

Lin, Z., Orlov, A., Lambert, R.M., Payne, M.C., 2005. J. Phy. Chem. B 109 (44), 20948-20952.

Liu, Y.-C., Yu, C.-C., Wang, C.-C., Juang, L.-C., 2006. Chem. Phys. Lett. 420 (1-3), 245-249.

Liu, Y., Lei, J., Huang, Y., Ju, H., 2014. Anal. Chem. 86 (17), 8735-8741.

Liu, Z., Chen, S., Liu, B., Wu, J., Zhou, Y., He, L., Ding, J., Liu, J., 2014. Anal. Chem. 86 (24), 12229-12235.

Mariathasan, S., Weiss, D.S., Newton, K., McBride, J., O'Rourke, K., Roose-Girma, M., Lee, W.P., Weinrauch, Y., Monack, D.M., Dixit, V.M., 2006. Nature 440 (7081), 228-232.

Mezhenny, S., Maksymovych, P., Thompson, T., Diwald, O., Stahl, D., Walck, S., Yates Jr, J., 2003. Chem. Phys. Lett. 369 (1-2), 152-158.

Miao, P., Tang, Y., Wang, L., 2017. ACS Appl. Mater. Interfaces 9 (4), 3940-3947.

Moskovits, M., 2005. J. Raman Spectrosc. 36 (6□7), 485-496.

Musumeci, A., Gosztola, D., Schiller, T., Dimitrijevic, N.M., Mujica, V., Martin, D., Rajh, T., 2009. J. Am. Chem. Soc. 131 (17), 6040-6041.

Ng, C., Cadusch, J.J., Dligatch, S., Roberts, A., Davis, T.J., Mulvaney, P., Gómez, D.E., 2016. ACS Nano 10 (4), 4704-4711.

Ng, Y.H., Lightcap, I.V., Goodwin, K., Matsumura, M., Kamat, P.V., 2010. J. Phy. Chem. Lett. 1 (15), 2222-2227.

Nian, J.-N., Teng, H., 2006. J. Phy. Chem. B 110 (9), 4193-4198.

Onda, K., Li, B., Petek, H., 2004. Phys. Rev. B 70 (4), 045415.

Pallaoro, A., Braun, G.B., Reich, N.O., Moskovits, M., 2010. Small 6 (5), 618-622.

Pei, H., Lu, N., Wen, Y., Song, S., Liu, Y., Yan, H., Fan, C., 2010. Adv. Mater. 22 (42), 4754-4758.

Qi, L., Xiao, M., Wang, F., Wang, L., Ji, W., Man, T., Aldalbahi, A., Khan, M.N., Periyasami, G., Rahaman, M., 2017. Nanoscale 9 (37), 14184-14191.

Qi, L., Xiao, M., Wang, X., Wang, C., Wang, L., Song, S., Qu, X., Li, L., Shi, J., Pei, H., 2017. Anal. Chem. 89 (18), 9850-9856.

Qian, X., Peng, X.-H., Ansari, D.O., Yin-Goen, Q., Chen, G.Z., Shin, D.M., Yang, L., Young, A.N., Wang, M.D., Nie, S., 2008. Nat. Biotechnol. 26 (1), 83-90.

Qu, X., Yang, F., Chen, H., Li, J., Zhang, H., Zhang, G., Li, L., Wang, L., Song, S., Tian, Y., 2017. ACS Appl. Mater. Interfaces 9 (19), 16026-16034.

Qu, X., Zhu, D., Yao, G., Su, S., Chao, J., Liu, H., Zuo, X., Wang, L., Shi, J., Wang, L., 2017. Angew. Chem. Int. Ed. 56 (7), 1855-1858.

Ramya, A.N., Joseph, M.M., Nair, J.B., Karunakaran, V., Narayanan, N., Maiti, K.K., 2016. ACS Appl. Mater. Interfaces 8 (16), 10220-10225.

Roseman, J.M., Lin, J., Ramakrishnan, S., Rosenstein, J.K., Shepard, K.L., 2015. Nat. Commun. 6 10070.

Shen, W., Li, M., Wang, B., Liu, J., Li, Z., Jiang, L., Song, Y., 2012. J. Mater. Chem. 22 (16), 8127-8133.

Stobiecka, M., 2014. Biosens. Bioelectron. 55, 379-385.

Stobiecka, M., Chalupa, A., 2015. J. Phy. Chem. B 119 (41), 13227-13235.

Stojanovic, M.N., De Prada, P., Landry, D.W., 2001. J. Am. Chem. Soc. 123 (21), 4928-4931.

Su, Y., Peng, T., Xing, F., Li, D., Fan, C., 2017. Acta Chim. Sinica 75 (11), 1036-1046.

Sudnik, L.M., Norrod, K.L., Rowlen, K.L., 1996. Appl. Spectrosc. 50 (3), 422-424.

Theiss, J., Pavaskar, P., Echternach, P.M., Muller, R.E., Cronin, S.B., 2010. Nano Lett. 10 (8), 2749-2754.

Tian, G., Fu, H., Jing, L., Xin, B., Pan, K., 2008. J. Phys. Chem. C 112 (8), 3083-3089.

Wan, Y., Lao, R., Liu, G., Song, S., Wang, L., Li, D., Fan, C., 2010. J. Phy. Chem. B 114 (19), 6703-6706.

Wan, Y., Xu, H., Su, Y., Zhu, X., Song, S., Fan, C., 2013. Biosens. Bioelectron. 41, 526-531.

Wang, C., Zhang, X., Zhang, Y., Jia, Y., Yang, J., Sun, P., Liu, Y., 2011. J. Phys. Chem. C 115 (45), 22276-22285.

Wang, G., Wang, Y., Chen, L., Choo, J., 2010. Biosens. Bioelectron. 25, 1859-1868.

Wang, K., Liao, J., Yang, X., Zhao, M., Chen, M., Yao, W., Tan, W., Lan, X., 2015. Biosens. Bioelectron. 63, 172-177.

Wang, X., Shi, W., She, G., Mu, L., 2012. Phy. Chem. Chem. Phy. 14 (17), 5891-5901.

Wang, Y., Yan, B., Chen, L., 2012. Chem. Rev. 113 (3), 1391-1428.

Wei, Y., Chen, Y., Li, H., Shuang, S., Dong, C., Wang, G., 2015. Biosens. Bioelectron. 63, 311-316.

Xu, C., Yang, X., Fu, X., Tian, R., Jacobson, O., Wang, Z., Lu, N., Liu, Y., Fan, W., Zhang, F., 2017. Adv. Mater. 29 (6), 1603673.

Yang, F., Zuo, X., Li, Z., Deng, W., Shi, J., Zhang, G., Huang, Q., Song, S., Fan, C., 2014. Adv. Mater. 26 (27), 4671-4676.

Yang, L., Liu, H., Wang, J., Zhou, F., Tian, Z., Liu, J., 2011. Chem. Commun. 47 (12), 3583-3585.

Yang, Q., Deng, M., Li, H., Li, M., Zhang, C., Shen, W., Li, Y., Guo, D., Song, Y., 2015. Nanoscale 7 (2), 421-425.

Ye, S., Xiao, J., Guo, Y., Zhang, S., 2013. Chem-Eur. J. 19 (25), 8111-8116.

Yoo, H., Bae, C., Yang, Y., Lee, S., Kim, M., Kim, H., Kim, Y., Shin, H., 2014. Nano Lett. 14 (8), 4413-4417.

Yoon, I., Kang, T., Choi, W., Kim, J., Yoo, Y., Joo, S.-W., Park, Q.-H., Ihee, H., Kim, B., 2008. J. Am. Chem. Soc. 131 (2), 758-762.

Zhang, J., Lao, R., Song, S., Yan, Z., Fan, C., 2008. Anal. Chem. 80 (23), 9029-9033.

Zhang, M., Chen, T., Liu, Y., Zhu, J., Liu, J., Wu, Y., 2019. Chemnanomat 5 (1), 55-60.

Zhang, X., Servos, M.R., Liu, J., 2012. J. Am. Chem. Soc. 134 (17), 7266-7269.

Zhao, B., Shen, J., Chen, S., Wang, D., Li, F., Mathur, S., Song, S., Fan, C., 2014. Chem. Sci. 5 (11), 4460-4466.

Zhong, R., Tang, Q., Wang, S., Zhang, H., Zhang, F., Xiao, M., Man, T., Qu, X., Li, L., Zhang, W., 2018. Adv. Mater. 30 (12), 1706887.

Zhou, C., Yu, Z., Yu, W., Liu, H., Zhang, H., Guo, C., 2019. Microchim. Acta 186 (4), 251.

Zuo, X., Song, S., Zhang, J., Pan, D., Wang, L., Fan, C., 2007. J. Am. Chem. Soc. 129 (5), 1042-1043.

Zuo, X., Xiao, Y., Plaxco, K.W., 2009. J. Am. Chem. Soc. 131 (20), 6944-6945.

Table of Contents

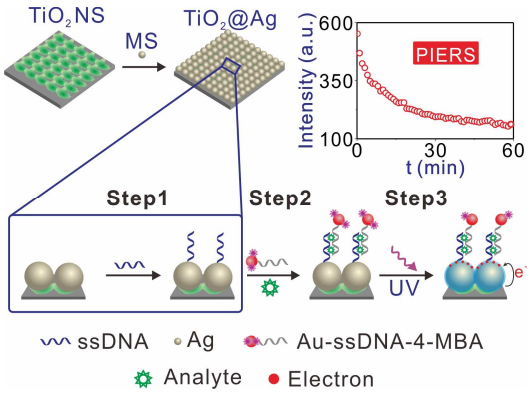

Highlights

A Versatile Biomolecular Detection Platform Based on Photo-Induced Enhanced Raman Spectroscopy

- A photo-induced enhanced Raman spectroscopy (PIERS) sensor was developed based on TiO_2@Ag.
- This PIERS sensor can detect various biomolecules with good specificity and high sensitivity.
- This versatile biomolecular detection platform shows promising potential for practical use.

Conflict of interest

A Versatile Biomolecular Detection Platform Based on Photo-Induced Enhanced Raman Spectroscopy

Conflict of interest

The authors declare no conflict of interest.

Declaration of interests

☒ The authors declare that they have no known competing financial interests or personal relationships that could have appeared to influence the work reported in this paper.

☐The authors declare the following financial interests/personal relationships which may be considered as potential competing interests: